Physics Letters B 770 (2017) 546–550

Contents lists available at ScienceDirect

Physics Letters B

www.elsevier.com/locate/physletb

Dirac CP phase in the neutrino mixing matrix and the Froggatt–Nielsen mechanism with $\det[M_\nu] = 0$

Yuya Kaneta [a,*], Morimitsu Tanimoto [b], Tsutomu T. Yanagida [c]

[a] Graduate School of Science and Technology, Niigata University, Niigata 950-2181, Japan
[b] Department of Physics, Niigata University, Niigata 950-2181, Japan
[c] Kavli Institute for the Physics and Mathematics of the Universe, University of Tokyo, Kashiwa 277-8583, Japan

ARTICLE INFO

Article history:
Received 5 February 2017
Received in revised form 12 April 2017
Accepted 8 May 2017
Available online 11 May 2017
Editor: J. Hisano

ABSTRACT

We discuss the Dirac CP violating phase δ_{CP} in the Froggatt–Nielsen model for a neutrino mass matrix M_ν imposing a condition $\det[M_\nu] = 0$. This additional condition restricts the CP violating phase δ_{CP} drastically. We find that the phase δ_{CP} is predicted in the region of $\pm(0.4\text{–}2.9)$ radian, which is consistent with the recent T2K and NOνA data. There is a remarkable correlation between δ_{CP} and $\sin^2\theta_{23}$. The phase δ_{CP} converges to $\sim \pm\pi/2$ if $\sin^2\theta_{23}$ is larger than 0.5. Thus, the accurate measurement of $\sin^2\theta_{23}$ is important for a test of our model. The effective mass m_{ee} for the neutrinoless double beta decay is predicted in the rage 3.3–4.0 meV.

1. Introduction

The Froggatt–Nielsen (FN) mechanism [1] is very attractive since it naturally explains the observed masses and mixing angles for quarks and leptons. It is well known that the magnitudes of observed mixing angles for quarks are given by powers of Wolfenstein parameter $\lambda \simeq 0.2$ [2]. This is nothing but the feature predicted by the FN mechanism. The lepton flavor mixing matrix, so called MNS matrix [3,4], exhibits two large mixing angles, and one rather small mixing angle of the order of Cabibbo angle. Surprisingly, this lepton mixing matrix is also explained by the FN mechanism [5–11].

Among various proposals, Ling and Ramond [10] presented a clear phenomenological discussion of neutrino masses and mixing angles in terms of Cabibbo angle $\lambda_C \simeq 0.225$ [12]. Their texture is still consistent with the recent precise data on the three neutrino mixing angles and two neutrino mass squared differences. However, this texture cannot predict the CP phase as we discuss later in this paper.

The neutrino oscillation experiments are now on a new step to confirm the CP violation in the lepton sector. Actually, the T2K and NOνA experiments indicate a finite CP phase [13–16]. Therefore, it is very interesting to extend the FN model to predict the Dirac CP violating phase.

In this paper, we discuss the Dirac CP violating phase in the FN model for the neutrino mass matrix M_ν imposing an additional condition $\det[M_\nu] = 0$ [17]. This flavor-basis independent condition of $\det[M_\nu] = 0$ is obtained easily by assuming two families of heavy right-handed neutrinos [18] in the framework of the seesaw mechanism [19,20]. It is also interesting that the Affleck–Dine scenario [21] for leptogenesis [22,23] requires the mass of the lightest neutrino to be $m_1 = 10^{-10}$ eV [24,25], which practically leads to our condition $\det[M_\nu] = 0$. We show that the phase δ_{CP} is predicted in a narrow region using the presently available data on the mass squared differences and the mixing angles.

In section 2, we discuss a texture of the neutrino mass matrix imposing $\det[M_\nu] = 0$ in the FN model, where neutrinos are supposed to be Majorana particles. In section 3, we show numerical results on δ_{CP}, $\sin^2\theta_{23}$, $\sin^2\theta_{13}$ and $\sin^2\theta_{12}$. The effective mass m_{ee} that appears in the neutrinoless double beta decay is also discussed. The summary and discussion are given in section 4.

2. FN texture for leptons

Let us discuss lepton mass matrices in the framework of the FN model. We assign the FN charges of the FN broken U(1) [1] to the three left-handed leptons ℓ_{Li} as

$$\ell_{L1}, \ell_{L2}, \ell_{L3} \ : \ n+1, n, n\,, \tag{1}$$

where n is a positive integer. Then, the mass matrix of the left-handed Majorana neutrinos is given in terms of the FN parameter λ, which is of the order of the Cabibbo angle λ_C, as follows:

* Corresponding author.
E-mail address: kaneta@muse.sc.niigata-u.ac.jp (Y. Kaneta).

http://dx.doi.org/10.1016/j.physletb.2017.05.025

$$M_\nu \sim \begin{pmatrix} \lambda^2 & \lambda & \lambda \\ \lambda & 1 & 1 \\ \lambda & 1 & 1 \end{pmatrix} . \tag{2}$$

This mass matrix leads to the Normal Hierarchy (NH) of neutrino masses, and gives us evidently one large mixing angle between the second and third families of neutrinos. Namely, the FN charge of the left-handed leptons is chosen by the observed large mixing. The charged lepton mass matrix is given after fixing FN charges of the right-handed charged leptons to reproduce the observed mass hierarchy among the charged leptons. Assigning FN charges to the three right-handed charged leptons e_{Ri} as

$$e_{R1}, e_{R2}, e_{R3} : 4, 2, 0 , \tag{3}$$

the charged lepton mass matrix M_E is given as

$$M_E \sim \begin{pmatrix} \lambda^5 & \lambda^3 & \lambda \\ \lambda^4 & \lambda^2 & 1 \\ \lambda^4 & \lambda^2 & 1 \end{pmatrix} , \tag{4}$$

which gives the mass ratio in terms of λ as follows:

$$\frac{m_e}{m_\tau} \sim \lambda^5 , \qquad \frac{m_\mu}{m_\tau} \sim \lambda^2 . \tag{5}$$

These mass ratios are consistent with observed ones for about $\lambda \simeq 0.2$.

We move to the diagonal basis of the charged lepton mass matrix in order to reduce the number of free parameters. Then, the rotation of the left-handed lepton doublets to diagonalize the charged lepton mass matrix does not change the powers of λ in the entries of the neutrino mass matrix of Eq. (2). Therefore, we discuss the following neutrino mass matrix in the diagonal basis of the charged lepton mass matrix:

$$M_\nu = m_0 \begin{pmatrix} a\lambda^2 & b\lambda & c\lambda \\ b\lambda & d & e \\ c\lambda & e & f \end{pmatrix} , \tag{6}$$

where $a - f$ are dimensionless complex parameters with their magnitudes of the order 1.[1]

By using the freedom of phase redefinition of the left-handed lepton fields, we take the diagonal elements to be real. Then, we have three CP phases in the mass matrix. Now, we parameterize the mass matrix in order to analyze the neutrino mixing numerically as

$$M_\nu = m_0 \begin{pmatrix} a\lambda^2 & b\lambda e^{i\phi_b} & c\lambda e^{i\phi_c} \\ be^{i\phi_b}\lambda & d & ee^{i\phi_e} \\ c\lambda e^{i\phi_c} & ee^{i\phi_e} & 1 \end{pmatrix} , \tag{7}$$

where $a - e$ are redefined as real parameters of the order 1.

Let us determine the magnitude of λ from the observed charged lepton mass ratios in Eq. (5). We use the m_e/m_τ ratio to fix λ, since it has the strongest λ dependence among charged lepton mass ratios as seen in Eq. (5). Then, we obtain $\lambda \simeq 0.20$ from the m_e/m_τ ratio. Taking into account the order one coefficients in those mass ratios in Eq. (5), $\lambda = 0.20$ can explain all lepton mass ratios consistently. We take $\lambda = 0.18 \sim 0.22$ considering the ambiguity of 10% for λ in our numerical computation.[2] We have now nine parameters m_0, $a - e$, ϕ_b, ϕ_c and ϕ_e, where the m_0 has dimension of a mass, but others are dimensionless parameters.

[1] Due to the rotation of the left-handed lepton doublets, the magnitude of the coefficients $a - f$ may be rather enlarged. We address this point in the section 4.

[2] The ambiguity of the coefficients $a - e$ due to the rotation of the left-handed lepton doublets is partially absorbed by taking account of the ambiguity of 10% for λ.

Table 1
Results of the global analysis of the neutrino oscillation experimental data for NH of neutrino masses [26], where observables are defined in Particle Data Group [12].

Observable	Best fit and 1σ	2σ interval
Δm^2_{23}	$2.524^{+0.039}_{-0.040} \times 10^{-3}$ eV^2	$(2.44 \sim 2.56) \times 10^{-3}$ eV^2
Δm^2_{12}	$7.50^{+0.19}_{-0.17} \times 10^{-5}$ eV^2	$(7.16 \sim 7.88) \times 10^{-5}$ eV^2
$\sin^2\theta_{23}$	$0.441^{+0.027}_{-0.021}$	$0.39 \sim 0.63$
$\sin^2\theta_{12}$	0.306 ± 0.012	$0.28 \sim 0.33$
$\sin^2\theta_{13}$	0.02166 ± 0.00075	$0.020 \sim 0.023$

Let us impose a flavor-basis independent condition that the determinant of the neutrino mass matrix vanishes, that is $\det[M_\nu] = 0$. This condition gives two constraints on the parameters, and then the neutrino mass matrix has now just seven free parameters which can be fully determined by future feasible experiments [17]. We see below that thanks to this condition, we can predict the CP violating phase δ_{CP}, which is defined in the Particle Data Group [12].

3. Numerical analysis

Let us present our numerical analysis of the neutrino mass matrix in Eq. (7). The free parameters $a - e$ are of the order one. We scan them in the region of $0.7 \sim 1.3$ by generating random numbers in the liner scale. Our choice of the parameter region of $0.7 \sim 1.3$ is justified later by the predicted mixing of $\sin^2\theta_{23}$. The parameter λ is essentially given by the FN model. As discussed in the previous section, the charged lepton mass hierarchy indicates $\lambda \simeq 0.2$. In our numerical analysis, we also scan it at random with the liner scale in the region $\lambda = 0.18 \sim 0.22$. Furthermore, the extension of the scanning region, for example, $0.5 \sim 2$ is not favored because the hierarchies between $a\lambda^2$ and $b\lambda(c\lambda)$, and between $b\lambda(c\lambda)$ and d, are no longer distinguishable, and then the FN scheme with $\lambda \simeq 0.2$ becomes meaningless.

The CP violating phases ϕ_b, ϕ_c and ϕ_e are also scanned in the full region of $-\pi \sim \pi$ by generating random numbers in the liner scale.

Now we explain how to obtain our predictions in our figures. By scanning the parameters of $a - e$ and three phases with $\lambda = 0.18 \sim 0.22$, we generate a neutrino mass matrix. The parameter m_0 is determined to reproduce the observed values of Δm^2_{23} and Δm^2_{12} at 2σ interval in Table 1. In practice, m_0 is also scanned randomly in the linear scale up to the upper bound of the total neutrino mass 0.2 eV, which is given by the cosmology observation [12]. Actually, the obtained m_0 is in the region of (0.025–0.035) eV. It is noticed, in the case of $\det[M_\nu] = 0$, m_0 is easily determined by the experimental data of Δm^2_{12} and Δm^2_{23} because of $m_1 = 0$.

Then, we obtain the calculated three mixing angles. If these predicted mixing angles are OK for the experimental data in Table 1, we keep the point. Otherwise, we disregard the point. We continue this procedure to obtain 10^4 points, which satisfy the experimental data.

3.1. Prediction of mixing angles

First, we discuss the mixing angle θ_{23} by imposing $\det[M_\nu] = 0$. This mass matrix leads to a large mixing angle θ_{23} naturally since all elements of the submatrix for the second and third families are of the order one. We can predict the magnitude of $\sin^2\theta_{23}$ by using only the experimental data Δm^2_{23} and Δm^2_{12} with 2σ error-bar in Table 1. We show the frequency distribution of the predicted $\sin^2\theta_{23}$ in Fig. 1, where $\lambda = 0.18 \sim 0.22$ and $a - e = 0.7 \sim 1.3$ are taken. It is remarkable that predicted $\sin^2\theta_{23}$ lies inside the

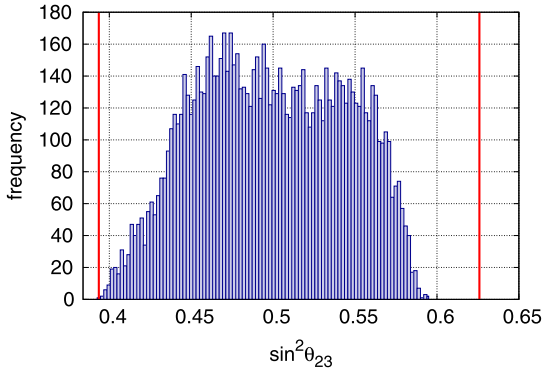

Fig. 1. The frequency distribution of the predicted $\sin^2\theta_{23}$ under the condition of $\det[M_\nu]=0$, where only the experimental data of Δm^2_{23} and Δm^2_{12} are input. The vertical red lines denote the observed $\sin^2\theta_{23}$ interval at 2σ. (For interpretation of the references to color in this figure legend, the reader is referred to the web version of this article.)

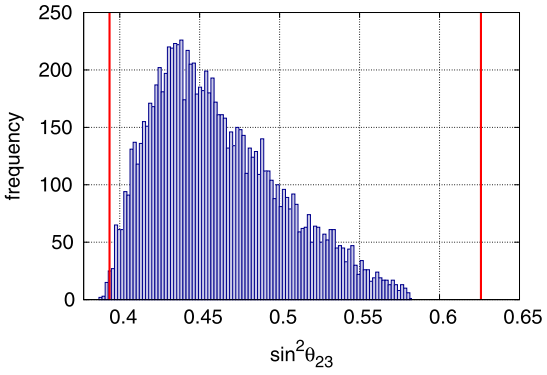

Fig. 2. The frequency distribution of the predicted $\sin^2\theta_{23}$ with adding the input data of $\sin^2\theta_{12}$ with 2σ error-bar, where the condition $\det[M_\nu]=0$ is imposed. The vertical red lines denote the observed $\sin^2\theta_{23}$ interval at 2σ. (For interpretation of the references to color in this figure legend, the reader is referred to the web version of this article.)

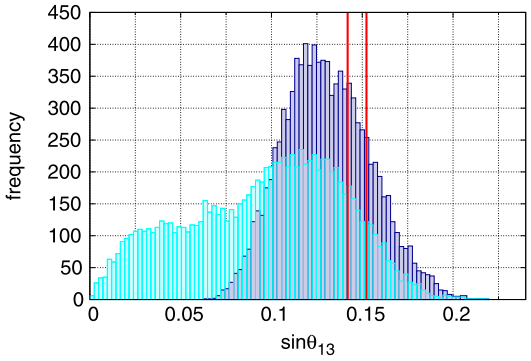

Fig. 3. The frequency distribution of the predicted $\sin\theta_{13}$, where the blue (cyan) corresponds to the case with (without) $\det[M_\nu]=0$. Only the experimental data of Δm^2_{23} and Δm^2_{12} are used as inputs. The vertical red lines denote the observed $\sin\theta_{13}$ interval at 2σ. (For interpretation of the references to color in this figure legend, the reader is referred to the web version of this article.)

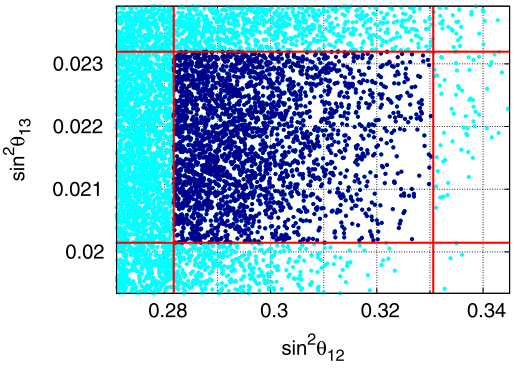

Fig. 4. The predicted region on the plane of $\sin^2\theta_{12}$ and $\sin^2\theta_{13}$ under the condition of $\det[M_\nu]=0$, where only the experimental data of Δm^2_{23} and Δm^2_{12} are used as inputs. The scattered plot is shown in the experimental allowed region with 3σ. The red lines denote the observed interval at 2σ. (For interpretation of the references to color in this figure legend, the reader is referred to the web version of this article.)

experimental allowed region of 2σ. The prediction almost distributes around 0.5 symmetrically. The predicted region of $\sin^2\theta_{23}$ depends on our choice of $a-e=0.7\sim1.3$. That is to say, our choice of $a-e=0.7\sim1.3$ nicely predicts $\sin^2\theta_{23}$ for the fixed $\lambda=0.18\sim0.22$. For example, an extension of the scanning region such as $a-e=0.5\sim1.5$ leads to $\sin^2\theta_{23}$ which lies over the experimental allowed region. This is a reason why we take $a-e=0.7\sim1.3$ in this paper.

Let us use the constraint from the data $\sin^2\theta_{12}$ with 2σ error-bar in Table 1 in addition to the data of Δm^2_{23} and Δm^2_{12}. The predicted $\sin^2\theta_{23}$ is shown in Fig. 2. The frequency distribution of $\sin^2\theta_{23}$ is remarkably changed. It is asymmetric around 0.5 as seen in Fig. 2. The region $\sin^2\theta_{23}<0.5$ is favored. It may be interesting to comment that this prediction is not changed even if the data of $\sin^2\theta_{13}$ is added. Thus, the input of $\sin^2\theta_{12}$ pushes $\sin^2\theta_{23}$ toward a region smaller than 0.5. It is interesting that the peak of the frequency distribution is around 0.44, which is the best fit value of the experimental data as seen in Table 1.

We add a comment that the distribution plot of Fig. 2 covers all region of the experimental interval of Δm^2_{23} and Δm^2_{12} in Table 1. It also covers all region of the experimental interval of $\sin^2\theta_{12}$ as seen later in Fig. 8.

The other mixing angles θ_{12} and θ_{13} are also predictable. We show the frequency distribution of the predicted $\sin\theta_{13}$ with/without imposing $\det[M_\nu]=0$ in Fig. 3, where only the experimental data of Δm^2_{23} and Δm^2_{12} are used as inputs. The tiny $\sin\theta_{13}$ is still allowed in spite of the $(1,3)$ matrix element being of the order λ in Eq. (7) unless the condition of $\det[M_\nu]=0$ is imposed. It is remarkable that the condition of $\det[M_\nu]=0$ excludes the smaller region than 0.07 for $\sin\theta_{13}$ as seen in Fig. 3. Thus, the condition of $\det[M_\nu]=0$ leads to $\sin\theta_{13}\simeq0.1$ naturally.

On the other hand, the predicted region of θ_{12} is rather broad. It is understandable that the $(1,2)$ entry of the neutrino mass matrix in Eq. (7) could be drastically reduced after the large rotation of the second and third family axes since both $(1,2)$ and $(1,3)$ entries are of the order λ. In particular, a large cancellation in the $(1,2)$ entry is required to satisfy the condition $\det[M_\nu]=0$, since the $(3,3)$ entry is much larger than the $(2,2)$ entry after the large rotation. In fact, the predicted region for $\sin^2\theta_{12}$ contains the region around 0. We present the predicted region on the plane of $\sin^2\theta_{12}$ and $\sin^2\theta_{13}$ with the condition of $\det[M_\nu]=0$ in Fig. 4, where the scattered plot is shown in the experimental allowed region with 3σ. It is concluded that the predicted θ_{12} and θ_{13} are completely consistent with the experimental data. Now, we try to predict the CP violating phase δ_{CP} in the next subsection.

3.2. Prediction of δ_{CP}

In order to predict the CP violating phase δ_{CP} precisely, we also use the data of all mixing angles, θ_{23}, θ_{12} and θ_{13}, in addition to Δm^2_{23} and Δm^2_{12}. At first, we show the calculated frequency distribution of δ_{CP} without imposing $\det[M_\nu]=0$ in Fig. 5. The vertical dashed lines denote the observed δ_{CP} interval at 90% C.L. in the

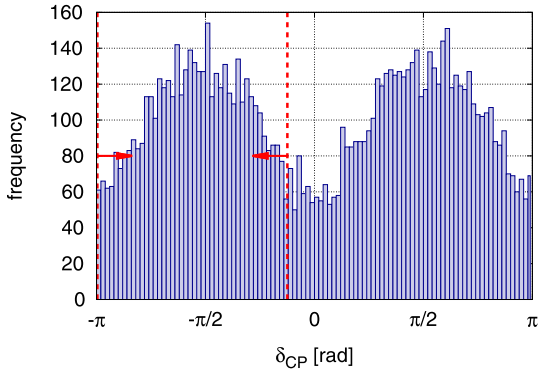

Fig. 5. The frequency distribution of the predicted δ_{CP} without $\det[M_\nu] = 0$. The vertical dashed lines denote the observed δ_{CP} interval at 90% C.L. in the T2K experiment [14].

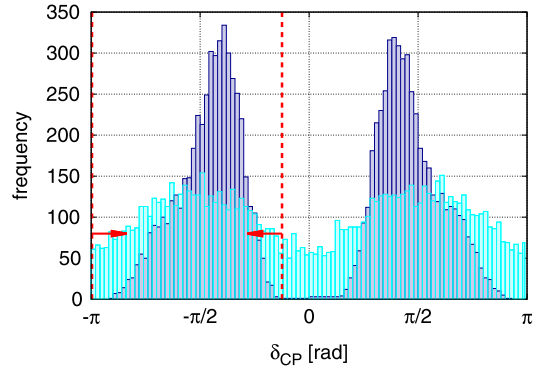

Fig. 6. The frequency distribution of the predicted δ_{CP}, where the blue (cyan) corresponds to the case with (without) $\det[M_\nu] = 0$. The vertical dashed lines denote the observed δ_{CP} interval at 90% C.L. in the T2K experiment [14]. (For interpretation of the references to color in this figure legend, the reader is referred to the web version of this article.)

recent T2K experiment [14]. We see that the predicted δ_{CP} lies in the all region $-\pi \sim \pi$.

However, when $\det[M_\nu] = 0$ is imposed on the neutrino mass matrix in Eq. (7), δ_{CP} is predicted around $\pm\frac{\pi}{2}$ as seen in Fig. 6, where blue (cyan) corresponds to the case with (without) $\det[M_\nu] = 0$. The CP conserved case $\delta_{CP} = 0, \pm\pi$ is excluded. The allowed region of δ_{CP} is $\pm(0.4 \sim 2.9)$ radian, which is consistent with the observed δ_{CP} interval $-(0.39 \sim 3.13)$ radian at 90% C.L. by using the Feldman–Cousins method for NH in the recent T2K experiment [14]. Thus, the condition of $\det[M_\nu] = 0$ is essential for the prediction of δ_{CP}.

We also discuss the correlations among mixing angle θ_{23} and CP violating phase δ_{CP}. We show the plot δ_{CP} versus $\sin^2\theta_{23}$ in Fig. 7, where $\det[M_\nu] = 0$ is imposed. As $\sin^2\theta_{23}$ increases, the predicted range of δ_{CP} becomes narrow. If $\sin^2\theta_{23}$ is larger than 0.5, δ_{CP} converges toward $\pm\pi/2$. Actually, the allowed region of δ_{CP} is $\pm(0.7 \sim 2.4)$ radian. More accurate measurements of $\sin^2\theta_{23}$ will be important to test our model.

We show the allowed region in the plane of $\sin^2\theta_{12}$ and $\sin^2\theta_{23}$ in Fig. 8, where $\det[M_\nu] = 0$ is imposed. The region where both of $\sin^2\theta_{12}$ and $\sin^2\theta_{23}$ are large is excluded.

3.3. Prediction of the effective mass m_{ee}

Finally, we discuss the effective neutrino mass responsible for the neutrinoless double beta decay

$$m_{ee} = \left| \sum_{i=2}^{3} m_i U_{ei}^2 \right| , \tag{8}$$

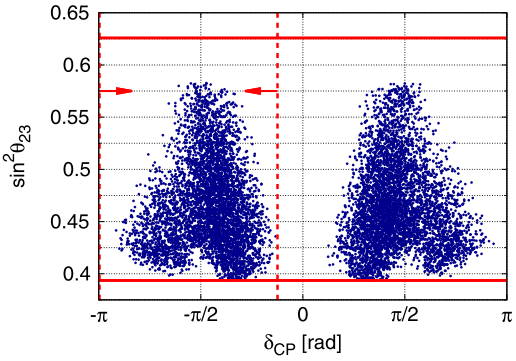

Fig. 7. The predicted δ_{CP} versus $\sin^2\theta_{23}$ with imposing $\det[M_\nu] = 0$. The horizontal red lines denote the experimental bounds for $\sin^2\theta_{23}$ with 2σ. The vertical dashed lines denote the observed δ_{CP} interval at 90% C.L. in the T2K experiment [14]. (For interpretation of the references to color in this figure legend, the reader is referred to the web version of this article.)

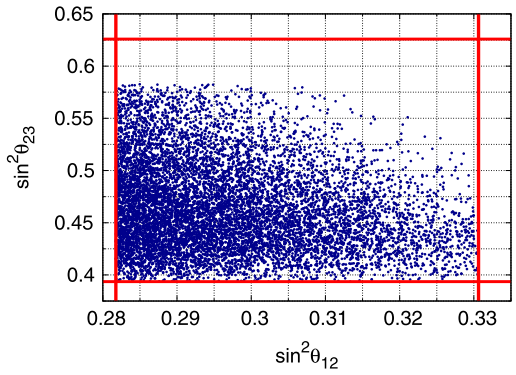

Fig. 8. The allowed region in the plane of $\sin^2\theta_{12}$ and $\sin^2\theta_{23}$ with imposing $\det[M_\nu] = 0$. The red lines denote the experimental bounds for $\sin^2\theta_{12}$ and $\sin^2\theta_{23}$ with 2σ. (For interpretation of the references to color in this figure legend, the reader is referred to the web version of this article.)

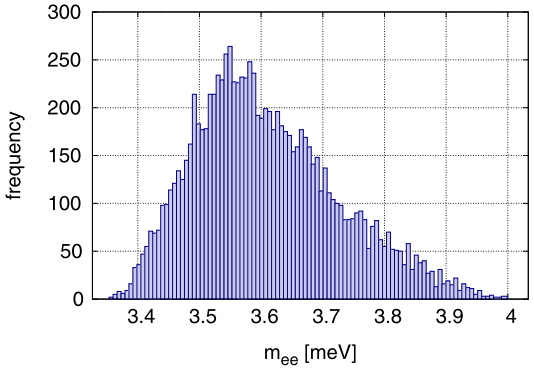

Fig. 9. The frequency distribution of the predicted m_{ee} with imposing $\det[M_\nu] = 0$.

where U_{ei} denotes the MNS mixing matrix element. We show the frequency distribution of the predicted m_{ee}, which lies in the range $m_{ee} = 3.35$–4.00 meV, in Fig. 9, where $\det[M_\nu] = 0$ is imposed.

4. Summary and discussion

We have discussed the mixing angles and the Dirac CP violating phase in the framework of the FN model with the flavor-basis independent condition $\det[M_\nu] = 0$. It is remarkable that $\sin^2\theta_{23}$ is predicted inside of the experimental allowed region of 2σ, where we have used only the data of Δm_{23}^2 and Δm_{12}^2. Here, we have taken the order one parameters to be $a - e = 0.7 \sim 1.3$ and the

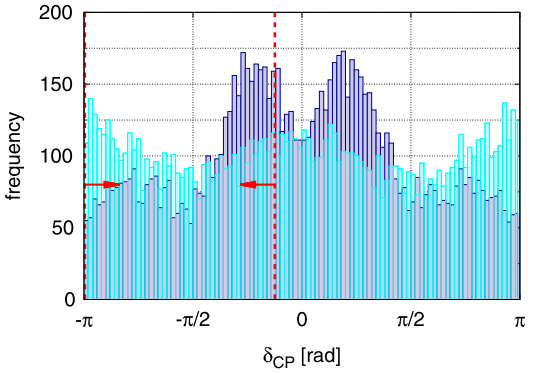

Fig. 10. The frequency distribution of the predicted δ_{CP} by scanning $a-e=0.5\sim 2$, where the blue (cyan) corresponds to the case with (without) $\det[M_\nu]=0$. The vertical dashed lines denote the observed δ_{CP} interval at 90% C.L. in the T2K experiment. (For interpretation of the references to color in this figure legend, the reader is referred to the web version of this article.)

FN parameter $\lambda=0.18\sim 0.22$. We have found that the predicted $\sin^2\theta_{13}$ and $\sin^2\theta_{12}$ are also completely consistent with the experimental data. Our numerical results depend on the scanning region $a-e=0.7\sim 1.3$. The condition of $\det[M_\nu]=0$ is essential for the nontrivial prediction of δ_{CP}. The allowed region of δ_{CP} is consistent with the recent T2K and NOνA data. The CP conservation $\delta_{CP}=0,\pm\pi$ is excluded.

In order to see the effect of the order one parameters $a-e$ on our prediction of δ_{CP}, we present the frequency distributions of δ_{CP} for $a-e=0.5\sim 2$ in Fig. 10. As the region of the parameter $a-e$ expands, the frequency distribution becomes broader. Notice that the hierarchies in the neutrino mass matrix M_ν predicted by the FN mechanism becomes obscure with such a large region of the parameters $a-e$ as stressed in section 3. In conclusion, we claim that $\det[M_\nu]=0$ predicts δ_{CP} as seen in Fig. 6 if the FN flavor structure is sharp.

It is helpful to comment on why $\det[M_\nu]=0$ rules out $\delta_{CP}=0,\pm\pi$ as seen in Fig. 6. The five neutrino experimental data, two mass squared differences and three mixing angles, are possibly reproduced by six parameters $a-e$ and m_0 without complex phases because of enough number of free parameters. Then, neutrino sector is the CP conserved one. When $\det[M_\nu]=0$ is imposed, we have five real parameters, and so we cannot reproduce the experimental data if $a-e$ are constrained around 1 without the CP violating phase. Thus, the CP conserved case $\delta_{CP}=0,\pm\pi$ is ruled out by the condition $\det[M_\nu]=0$.

The condition of $\det[M_\nu]=0$ is derived easily by assuming two families of heavy right-handed neutrinos in the framework of the seesaw mechanism. Notice that the neutrino mass matrix M_ν in Eq. (2) is determined only by the FN charges of the left-handed leptons after the integration of the right-handed neutrinos.

It is emphasized that the scenario with the two family heavy right-handed neutrinos is not necessarily required. In practice, we have checked that our prediction of δ_{CP} is not changed in the case of m_1 being smaller than 10^{-4} eV. However, we do not address the model with tiny m_1 since it is beyond the scope of our work.

We have also found the remarkable correlation between δ_{CP} and $\sin^2\theta_{23}$. If $\sin^2\theta_{23}$ is larger than 0.5, δ_{CP} converges to around $\pm\pi/2$. We expect the accurate measurement of $\sin^2\theta_{23}$ will be done in near future experiments. The effective mass in the neutrinoless double beta decay m_{ee} is also predicted to be $m_{ee}=$ 3.3–4.0 meV.

We should note that our results are consistent with the conclusions in [27], where an exchange symmetry between two heavy right-handed neutrinos is further imposed. The CP violating phase δ_{CP} is predicted near by the maximal value $\pm\frac{\pi}{2}$ due to the exchange symmetry.

Acknowledgements

We thank G. Branco for careful reading of the manuscript. This work is supported by JSPS Grants-in-Aid for Scientific Research 15K05045, 16H00862 (MT) and 26287039, 26104009, 16H02176 (TTY). This work receives a support at IPMU by World Premier International Research Center Initiative of the Ministry of Education in Japan.

References

[1] C.D. Froggatt, H.B. Nielsen, Nucl. Phys. B 147 (1979) 277, http://dx.doi.org/10.1016/0550-3213(79)90316-X.
[2] L. Wolfenstein, Phys. Rev. Lett. 51 (1983) 1945, http://dx.doi.org/10.1103/PhysRevLett.51.1945.
[3] Z. Maki, M. Nakagawa, S. Sakata, Prog. Theor. Phys. 28 (1962) 870.
[4] B. Pontecorvo, Sov. Phys. JETP 26 (1968) 984, Zh. Eksp. Teor. Fiz. 53 (1967) 1717.
[5] W. Buchmuller, T. Yanagida, Phys. Lett. B 445 (1999) 399, http://dx.doi.org/10.1016/S0370-2693(98)01480-4, arXiv:hep-ph/9810308.
[6] F. Vissani, J. High Energy Phys. 9811 (1998) 025, http://dx.doi.org/10.1088/1126-6708/1998/11/025, arXiv:hep-ph/9810435.
[7] F. Vissani, Phys. Lett. B 508 (2001) 79, http://dx.doi.org/10.1016/S0370-2693(01)00485-3, arXiv:hep-ph/0102236.
[8] J. Sato, T. Yanagida, Phys. Lett. B 493 (2000) 356, http://dx.doi.org/10.1016/S0370-2693(00)01153-9, arXiv:hep-ph/0009205.
[9] J.K. Elwood, N. Irges, P. Ramond, Phys. Rev. Lett. 81 (1998) 5064, http://dx.doi.org/10.1103/PhysRevLett.81.5064, arXiv:hep-ph/9807228.
[10] F.S. Ling, P. Ramond, Phys. Lett. B 543 (2002) 29, http://dx.doi.org/10.1016/S0370-2693(02)02388-2, arXiv:hep-ph/0206004.
[11] M. Bando, N. Maekawa, Prog. Theor. Phys. 106 (2001) 1255, http://dx.doi.org/10.1143/PTP.106.1255, arXiv:hep-ph/0109018.
[12] C. Patrignani, et al., Particle Data Group, Chin. Phys. C 40 (10) (2016) 100001, http://dx.doi.org/10.1088/1674-1137/40/10/100001.
[13] K. Abe, et al., T2K Collaboration, Phys. Rev. Lett. 112 (18) (2014) 181801, http://dx.doi.org/10.1103/PhysRevLett.112.181801, arXiv:1403.1532 [hep-ex].
[14] K. Abe, et al., T2K Collaboration, arXiv:1701.00432 [hep-ex].
[15] P. Adamson, et al., NOvA Collaboration, Phys. Rev. Lett. 116 (15) (2016) 151806.
[16] J. Bian, arXiv:1611.07480 [hep-ex].
[17] G.C. Branco, R. Gonzalez Felipe, F.R. Joaquim, T. Yanagida, Phys. Lett. B 562 (2003) 265, http://dx.doi.org/10.1016/S0370-2693(03)00572-0, arXiv:hep-ph/0212341.
[18] P.H. Frampton, S.L. Glashow, T. Yanagida, Phys. Lett. B 548 (2002) 119, http://dx.doi.org/10.1016/S0370-2693(02)02853-8, arXiv:hep-ph/0208157.
[19] P. Minkowski, Phys. Lett. B 67 (1977) 421.
[20] T. Yanagida, Workshop on the Unified Theory and Baryon Number in the Universe, KEK report KEK-79-18, 1979, Conf. Proc. C 7902131, p. 95;
M. Gell-Mann, P. Ramond, R. Slansky, Supergravity, in: P. van Niewwenhuizen, D.Z. Freedman (Eds.), 1979, p. 315, Conf. Proc. C 790927, p. 315.
[21] I. Affleck, M. Dine, Nucl. Phys. B 249 (1985) 361, http://dx.doi.org/10.1016/0550-3213(85)90021-5.
[22] H. Murayama, T. Yanagida, Phys. Lett. B 322 (1994) 349, http://dx.doi.org/10.1016/0370-2693(94)91164-9, arXiv:hep-ph/9310297.
[23] M. Dine, L. Randall, S.D. Thomas, Nucl. Phys. B 458 (1996) 291, http://dx.doi.org/10.1016/0550-3213(95)00538-2, arXiv:hep-ph/9507453.
[24] T. Asaka, M. Fujii, K. Hamaguchi, T. Yanagida, Phys. Rev. D 62 (2000) 123514, http://dx.doi.org/10.1103/PhysRevD.62.123514, arXiv:hep-ph/0008041.
[25] M. Fujii, K. Hamaguchi, T. Yanagida, Phys. Rev. D 64 (2001) 123526, http://dx.doi.org/10.1103/PhysRevD.64.123526, arXiv:hep-ph/0104186.
[26] I. Esteban, M.C. Gonzalez-Garcia, M. Maltoni, I. Martinez-Soler, T. Schwetz, arXiv:1611.01514 [hep-ph].
[27] T. Rink, K. Schmitz, T.T. Yanagida, arXiv:1612.08878 [hep-ph].